Photo-stability of peptide-bond aggregates: N-methylformamide dimers.

Crespo-Otero, R; Mardykov, A; Sanchez-Garcia, E; Sander, W; Barbatti, M

PCCP

PAPER

View Article Online
View Journal | View Issue

Cite this: *Phys. Chem. Chem. Phys.*, 2014, **16**, 18877

Photo-stability of peptide-bond aggregates: *N*-methylformamide dimers†

Rachel Crespo-Otero,*[ab] Artur Mardykov,[c] Elsa Sanchez-Garcia,[a] Wolfram Sander*[c] and Mario Barbatti*[a]

Received 7th June 2014,
Accepted 24th July 2014

DOI: 10.1039/c4cp02518k

www.rsc.org/pccp

The formation of weakly-bound dimers of *N*-methylformamide (NMF) and the photochemistry of these dimers after irradiation at 248 nm were explored using matrix-isolation spectroscopy. Calculations were used to characterize the diverse isomers and assign their IR spectra; non-adiabatic dynamics was simulated to understand their photo-deactivation mechanism. The most stable dimers, ***tt-1*** and ***tt-2***, were obtained by *trans–trans* aggregation (N–H···O=C interactions) and could be identified in the matrix. The main products formed after irradiation are the *trans–cis* dimers (***tc-3*** and ***tc-4***), also stabilized by N–H···O=C interactions. In contrast to the photochemistry of the monomers, no dissociative products were observed after 248 nm irradiation of the dimers. The absence of dissociative products can be explained by a proton-transfer mechanism in the excited state that is faster than the photo-dissociative mechanism. The fact that hydrogen bonding has such a significant effect on the photochemical stability of NMF has important implications to understand the stability of peptide-bonded systems to UV irradiation.

Introduction

The study of the photochemistry of peptide systems is essential to understand the effect of UV irradiation on proteins and other biological systems.[1] Previously, we reported on the photochemistry of the *N*-methylformamide (NMF) monomer, which is the simplest peptide model that shows *cis–trans* isomerism.[2] *trans* NMF is thermodynamically more stable than *cis* being the dominant form in the gas phase and low-temperature matrices. Prolonged irradiation of *trans* NMF with laser of 248 nm in matrix-isolation conditions generates the *cis* isomer, CH_3NH_2 and CO as major products. The initially populated nπ* excited state is deactivated through a mechanism that involves the formation of the CH_3NH and HCO radicals as intermediates. Similar dissociative photochemistry has been reported for formamide and other small amides.[2–4] Here, we show that hydrogen-bonded NMF dimers are stable to UV irradiation in similar conditions due to a protective proton-transfer mechanism.

NMF dimers have been extensively studied both experimentally and theoretically.[5,6] The high-resolution IR spectrum of the NMF dimer in the gas phase was obtained by Suhm *et al.*[7] From the analysis of the N–H and C=O carbonyl stretches and their shifts, they concluded that the most stable T-shape *trans–trans* NMF dimer is formed. The aggregation of NMF in liquid thin films on AgX (X = CI or Br) planar fibers was investigated by Kosower *et al.*[8] In the initial steps (low concentrations, 0.1 s), monomers, dimers and trimers were detected. In another study, Shin *et al.*[9] carried out an IR spectroscopic study in an argon matrix for a preliminary conformational analysis of the dimers.

Proton-transfer mechanisms play an important role in the non-radiative deactivation of photo-excitation of different molecular systems. Experiments and theoretical calculations analyzed this mechanism in different peptide models.[10–15] The excitation decays through a conical intersection, producing an unstable ground-state tautomer, and the proton is transferred back preserving the original structure. If the process is fast enough, it can prevent photo-dissociative mechanisms and protect the original structure. In this context, the comparison with the photochemistry of the corresponding isolated molecule provides the framework to understand the role of the hydrogen-bonded systems on the stability of more complex biological structures to UV irradiation.

Marazzi *et al.*[13] analyzed the mechanism of deactivation of a glycine dimer after photo-population of the bright ππ* local excitations. The role of the nπ* local excitations on the deactivation process was discarded based on a high proton-transfer barrier. In contrast, we found that the mechanism of deactivation

[a] *Max-Planck-Institut für Kohlenforschung, Kaiser-Wilheim-Platz 1, 45470 Mülheim an der Ruhr, Germany. E-mail: barbatti@kofo.mpg.de*
[b] *Department of Chemistry, University of Bath, Claverton Down, Bath, BA1 7AY, UK. E-mail: r.crespo-otero@bath.ac.uk*
[c] *Lehrstuhl für Organische Chemie II, Ruhr Universität Bochum, Universitätsstraße 150, 44801 Bochum, Germany. E-mail: wolfram.sander@rub.de*
† Electronic supplementary information (ESI) available. See DOI: 10.1039/c4cp02518k

from the nπ* excited states of the hydrogen-bonded NMF dimers also involves the forward–backward proton-transfer mechanism.

Here, we use experimental and theoretical techniques to demonstrate that H-bonded interactions protect the NMF dimers from photo-dissociation. Matrix-isolation experiments allow identifying the stable dimers of NMF in argon matrix and the products obtained after UV irradiation (248 nm). Theoretical calculations are used for the interpretation of IR experiments and the assignment of dimers and photoproducts. Non-adiabatic dynamics simulations provide very useful information to understand photo-phenomena.[16] In particular, TD-DFT methods and surface hopping approaches are tailored for the description of photo-processes in relatively large-sized systems.[17–19] The competition between CN dissociation and proton-transfer mechanisms, as well as the distribution between different reaction channels, is addressed with these methods.

Experimental section

N-Methylformamide was obtained from Aldrich (>99% purity), dried over molecular sieves (4 Å), and degassed several times by the freeze–pump–thaw method. Matrix-isolation experiments were conducted by standard techniques using an APD CSW-202 Displex closed cycle helium refrigerator. Matrices were produced by co-deposition of NMF with a large excess of argon (Messer Griesheim, 99.99%) on top of a cold CsI window with a rate of approximately 0.11 mmol min^{-1}. NMF was evaporated from a glass tube kept at −30, −40, or −50 °C to control its vapor pressure. In a second set of experiments 600–800 mbar of argon were premixed with 0.5–1 mbar of NMF in a stainless steel flask. The flask was kept at 80 °C to avoid condensation of the NMF. The aggregation of NMF was achieved either by warming the matrix (argon) from 10 K to 40 K with a rate of approximately 1 K min^{-1} (free warm-up) or by annealing the matrix at a defined temperature between 20 and 40 K for up to 60 min. After the matrices were cooled back to 10 K, the spectra were recorded on a Bruker IFS spectrometer with 0.5 cm^{-1} resolution in the range between 400 and 4000 cm^{-1}. Laser photolysis processes were accomplished with a Compex100 Excimer-Laser (Lambda Physik LPX 105 SD) for l = 248 nm (Kr/F2).

Computational details

The IR spectra of NMF dimers generated under various conditions of deposition and annealing of matrices were compared with the calculated spectra at the B3LYP-D3/aug-cc-pVTZ level of theory. The inclusion of van der Waals corrections (D3)[20] is needed to describe the energetic of formation of these weak complexes. Several dimer structures with the monomers in the *cis* and *trans* configurations were computed. To facilitate the comparison between experimental and calculated shifts, the computed wavenumbers were scaled with individual factors obtained from the monomers (Table 1).

While our previous study of the dynamics of the NMF monomer was performed mainly using CASSCF, the study of the dimers was carried out with the TDDFT method. The main problem associated to the non-adiabatic dynamics simulations at the CASSCF level of theory is the selection of a consistent active space that represents properly all the photochemical channels involved. For the NMF dimers, where CN dissociative and proton-transfer processes are relevant, the active space must include the bonding and anti-bonding CN orbitals on each monomer, and the relevant lone pairs associated to the proton transfer process, which is computationally unfeasible. In addition, previous studies have shown the necessity of including electron correlation to describe properly proton-transfer processes.[21] Thus, the non-adiabatic dynamics simulations of the NMF dimers were performed with TDDFT.

Table 1 Experimental and calculated vibrational wavenumbers κ (in cm^{-1}) of the NMF monomers

	Monomers and factor of corrections						
	trans			*cis*			
Mode	κ calc.[a]	κ expt.	CF	κ calc.[a]	κ expt.	CF	Average CF
N–H wag.	542.3	535.5	0.99	607.6	602.1	0.99	0.99
C^{m}–N str.	946.7	947.7	1.00	1005.0	1000.9	0.99	0.99
C–N str.	1216.4	1205.5	0.99	1299.5	1292.9	0.99	0.99
C═O str.	1763.6	1725.4	0.98	1769.7	1730.6	0.98	0.98
N–H str.	3623.7	3493.7	0.96	3587.1	3456.4	0.96	0.96

[a] Vibrational wavenumbers of NMF monomers calculated at the B3LYP-D3/aug-cc-pVTZ level of theory. CF – correction factor.

An appropriate description of the charge-transfer (CT) states is needed for studying the coupling between hydrogen- and electron-transfer processes. It is well known that traditional DFT functionals have problems to describe CT states.[22] Long-range-separated functionals are good alternatives in this context.[23,24] The TD/LC-BLYP/6-311+G(d) level of theory was used to perform the non-adiabatic dynamics simulations. The range-separation parameter was fixed at $\mu = 0.2a_0^{-1}$, a value based on a non-empirical parameterization.[24]

To locate the intersection between S_0 and S_1, relaxed scans in S_1 were performed at the TD/LC-BLYP(μ = 0.2)/6-311+G(d) level of theory along the most relevant reaction coordinates. Structures with the minimum energy gap along these scans were taken as representatives of the intersection seam. Linear interpolations in the internal coordinate spaces from the Franck–Condon or the S_1 minima geometries to the S_1/S_0-crossing structures were performed for the isomer ***tt-1***.

To assess the performance of the selected functional, the linear interpolation pathways were recomputed using multi-state complete active space perturbation theory to the second order (MS-CASPT2) and the algebraic diagrammatic construction to the second order (ADC(2)),[25,26] both with the aug-cc-pVDZ basis set. For CASPT2, the active space included the whole π system (4π and 2π*), the two nonbonding pairs on the N atoms, and a pair of σ(C–N), σ*(C–N) orbitals on A or B depending on the breaking process that was simulated. This active space totalized 14 electrons in 10 orbitals [MS-PT2//CASSCF(14,10)].

Non-adiabatic dynamics simulations for NMF dimers in the gas phase were performed with a maximum simulation time of

1000 fs at the TD/LC-BLYP(μ = 0.2)/6-311+G(d) level of theory. Ground and three excited states were considered in the dynamics. The initial conditions were sampled from the simulated absorption spectrum to simulate a nearly monochromatic excitation.[27] A total of 101 trajectories were computed, 50 for the ***tt-1*** isomer and 51 for the ***tt-2*** isomer. Trajectories were integrated with a 0.5 fs time step for the classical equations and 0.025 fs for the quantum equations. The number of trajectories initiated in each state is discussed later. Non-adiabatic effects between excited states were included with the fewest-switches surface hopping[28] with decoherence corrections.[29] Linear-response TDDFT is not adequate to compute hops between the excited and the ground states. For this reason, we took as a measure of the internal conversion time, the time when the energy gap between S_1 and S_0 drops below 0.1 eV.

The MS-PT2 calculations were carried out using the MOLCAS program,[30] the B3LYP-D3 and ADC(2) calculations with Turbomole.[31] All TDDFT calculations were performed using Gaussian.[32] The Newton-X program[33,34] interfaced to Gaussian[32] was used to perform non-adiabatic simulations.[35]

To analyze the character of the excited states (localized or CT) of all structures along the selected proton transfer trajectory and all initial condition geometries, the excited-state electron densities were examined using a partition scheme based on contributions of the monomer fragments.[27,36]

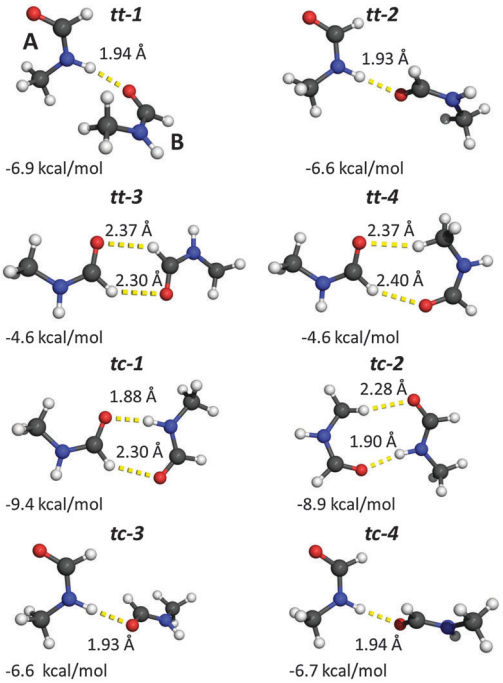

Fig. 1 *trans–trans* and *trans–cis* dimers identified in the matrix-isolation experiments. Stabilization energies computed at the B3LYP-D3/aug-cc-pVTZ including zero-point energy correction.

Results and discussion

Experiments

Dimer structures. Under the present experimental conditions, three types of NMF dimers can be formed: *trans–trans*, *trans–cis* and *cis–cis* (***tt***, ***tc***, and ***cc***, respectively). Fifteen dimers were considered (***tt***: 5, ***tc***: 7, ***cc***: 3), the stabilization energies and the structures of all of them are shown in the ESI† (Fig. 1S–3S and Table 1S). In all cases, the most stable complexes are stabilized by at least one N–H···O=C interaction. Additional C=O···H–C interactions involving the methyl or aldehyde H–C groups are present in many complexes.

The ***tt-1***, ***tt-2***, ***tt-3***, ***tt-4***, ***tc-1***, ***tc-2***, ***tc-3*** and ***tc-4*** complexes could be identified either after the aggregation or photochemistry experiments (Fig. 1, IR properties in Tables 2 and 3; Tables 2S and 3S, ESI†). The ***tt-1***, ***tt-2***, ***tc-3*** and ***tc-4*** complexes are mainly stabilized by the N–H···O=C interaction, showing intermolecular O–H distances between 1.88 and 1.94 Å. For these complexes, we use the following notation: monomer A is the hydrogen-bond donor (N–H), while monomer B is the hydrogen-bond acceptor (O=C). The ***tc-1*** and ***tc-2*** complexes, which are cyclic, have two stabilizing interactions: N–H···O=C and C–H···O=C. The ***tt-3*** and ***tt-4*** dimers are bound by C–H···O=C interactions, being the less stable of all considered structures.

The most stable dimer, ***cc-1***, was not identified in the matrix-isolation experiments because of the small concentration of the *cis* monomer during the aggregation experiments. The isomer ***cc-1*** is stabilized by two strong N–H···O=C interactions, resulting in a stabilization of −16.5 kcal mol^{-1} with respect to the isolated monomers. This value is almost twice the stabilization energy of the complexes ***tt-1*** (−7.9 kcal mol^{-1}), ***tt-2*** (−7.6 kcal mol^{-1}), ***tc-3*** (−7.7 kcal mol^{-1}) and ***tc-4*** (−7.7 kcal mol^{-1}), which feature only one N–H···O=C interaction.

Table 2 Experimental (argon matrix) and calculated vibrational wavenumbers κ and shifts $\Delta\kappa$ (in cm^{-1}) of the ***tt-1*** and ***tt-2*** dimers. All the calculated wavenumbers were scaled using the average correction factors shown in Table 1

		B3LYP-D3/aug-cc-pVTZ				
Experimental argon (cm^{-1})		***tt-1***		***tt-2***		
κ	$\Delta\kappa$	κ	$\Delta\kappa$	κ	$\Delta\kappa$	Assign.
952.9	+5.4	951.7	+6.9	948.7	+3.9	C^m–N str.
956.3	+8.8	966.5	+21.7	963.6	+18.8	
1219.2	+13.7	1230.1	+22.2	1225.5	+17.6	C–N str.
1227.5	+22.0	1251.0	+43.1	1250.4	+42.5	
1702.4	−23.0	1701.3	−23.5	1699.1	−25.7	C=O str.
1711.7	−13.7	1710.6	−14.2	1712.4	−12.4	
3411.6	−82.0	3363.7	−129.6	3331.6	−161.7	N–H str.
3477.9	−15.8	3502.8	+9.5	3492.1	−1.2	

Dimer formation. Two types of experiments were performed: (i) NMF was sublimed from a sample kept at −50 °C and deposited with a large excess of argon at temperatures of 15–30 K. Under these conditions, monomer M-*trans* was almost exclusively found. (ii) NMF was sublimed at −20 °C, where its vapor pressure is considerably higher. Again, monomer M-*trans* is the main product, but additional IR bands associated to the ***tt-1*** and ***tt-2*** dimers were also detected (Fig. 2). The presence of these complexes is evident from the C=O stretching vibrations at 1711.7 and 1702.4 cm^{-1} and other characteristic absorptions in the matrix IR spectra (Table 2).

Table 3 Experimental (argon matrix) and calculated vibrational wavenumbers κ and shifts $\Delta\kappa$ (in cm^{-1}) of the ***tc-3*** and ***tc-4*** dimers (the shifts were computed with respect to the *cis* monomer). All the calculated wavenumbers were scaled using the factors shown in Table 1

		B3LYP-D3/aug-cc-pVTZ				
Experimental argon (cm^{-1})		***tc-3***		***tc-4***		
κ	$\Delta\kappa$	κ	$\Delta\kappa$	κ	$\Delta\kappa$	Assign.
621.5[a]	+19.4	637.8	+36.2	637.4	+35.8	N–H wag.
712.7	+110.6	727.2	+125.6	722.6	+121.1	
967.1	−33.8	964.7	−38.3	963.3	−39.7	C^m–N str.
1008.4[a]	+7.5	1008.9	+5.9	1007.7	+4.7	
		1251.5	−38.9	1248.9	−41.5	C–N str.
1317.7[a]	+24.8	1313.7	+23.3	1313.4	+23.0	
1692.1	−38.5	1704.8	−26.0	1704.1	−26.7	C═O str.
1710.9[a]	−19.7	1716.2	−14.6	1715.2	−15.6	
3396.6	−59.8	3327.8	−130.1	3332.9	−125.0	N–H str.
		3454.7	−3.3	3454.3	−3.7	

[a] Vibrational modes of the *cis*-conformer of NMF.

The aggregation experiments were carried out by either warming the argon matrices from 10 to 40 K with a rate of approximately 1 K min^{-1} (free warm-up, Fig. 2) or by annealing the matrix at a defined temperature between 20 and 40 K for up to 60 min (Fig. 4S, ESI†). Most of the new signals formed during the aggregation are associated to ***tt*** dimers, since the concentration of *cis*-NMF monomer in the matrix is very low. Under both conditions – free warm-up and annealing of the matrix – new signals appearing can be assigned to the complexes ***tt-1*** and ***tt-2***. These isomers are structurally and energetically similar (−6.9 and −6.6 kcal mol^{-1} after zero point energy correction), and correspond to analogous complexes reported in the aggregation of *N*-methylacetamide.[37] Our assignment is also in agreement with previous reports of supersonic jet expansion experiments.[7] Additional signals can be assigned to small amounts of the ***tt-3*** and ***tt-4*** dimers, stabilized only by weaker C–H···O═C interactions. Several weak signals are tentatively assigned to complexes between *cis*-NMF (present in very low concentration) and *trans*-NMF (***tc-1*** and ***tc-2*** dimers).

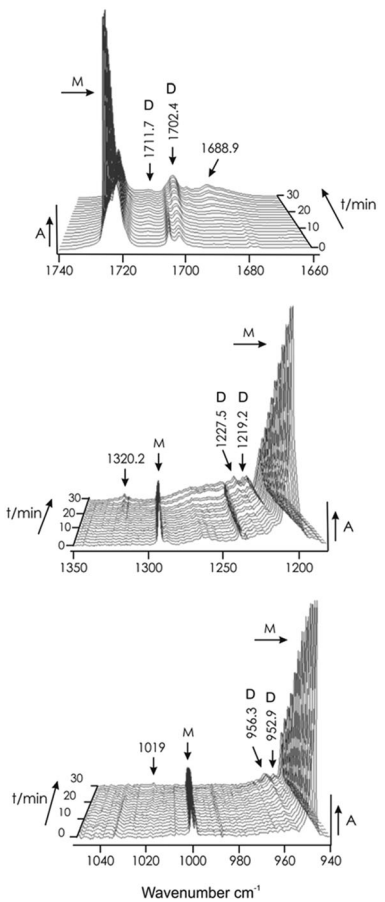

Fig. 2 IR spectra of an argon matrix containing NMF during slow warming from 10 K (t = 0) to 40 K (t = 30 min). M: bands of monomeric NMF, D: bands of the NMF dimers. D signals correspond to the ***tt-1*** and ***tt-2*** dimers.

Photochemistry of the NMF dimers. UV irradiation (λ = 248 nm) of an argon matrix containing *trans*-NMF and the *trans–trans* dimers (***tt-1*** and ***tt-2***) resulted in the decrease of all IR absorptions assigned to these species (Fig. 3) and formation of new bands at 3396.6, 1710.9, 1317.7, 1008.4, 712.7 and 621.5 cm^{-1}. Some of these bands appear close to bands of *cis*-NMF, indicating that the formed dimers contain at least one *cis*-NMF. These bands appear only if the dimers ***tt-1*** and ***tt-2*** are present in the matrix and, based on DFT calculations, are assigned to ***tc-3*** and ***tc-4*** (Fig. 3 and Table 3). Although the ***tc-3*** and ***tc-4*** are not the lowest-energy ***tc*** dimers, their formation is strongly supported by the comparison between computed and experimental IR spectra.

Interestingly, our experiments reveal that the *trans–cis* photoisomerization in dimers ***tt-1*** and ***tt-2*** occurs only in the NMF molecule acting as hydrogen-bond acceptor, whereas the donor NMF molecule does not undergo isomerization. The formation of both complexes ***tc-3*** and ***tc-4*** in the argon matrix seems to be the consequence of a single isomerization step of ***tt-1*** and ***tt-2*** dimers. It suggests possible isomerization mechanisms:

$$\textbf{\textit{tt-1}} \rightarrow \textbf{\textit{tc-3}}, \quad (1)$$

$$\textbf{\textit{tt-2}} \rightarrow \textbf{\textit{tc-4}}, \quad (2)$$

which require only a *trans* to *cis* conformational change in the acceptor NMF molecule. The formation of the energetically more favorable heterodimers (for example ***tc-1*** and ***tc-2***) was not observed in our experiments.

The photo-dissociation of NMF leads to CH_3NH_2, CO and *N*-methylformimidic acid, which are also formed during the 248 nm irradiation of matrices containing mixtures of the NMF monomer and dimers as described above (Fig. 3).[2] Most notably, the dimers are found to be very stable towards UV irradiation and do not decompose to CH_3NH_2 and CO under conditions while the NMF monomer rapidly photolyzed. Non-adiabatic dynamics simulations (see below) have been performed to explain the absence of dissociative photochemistry in the dimers.

Calculations

Excited states: vertical spectrum. The excitation energies calculated with TDDFT are in very good agreement with the ADC(2) results (Table 4). The root mean square deviation

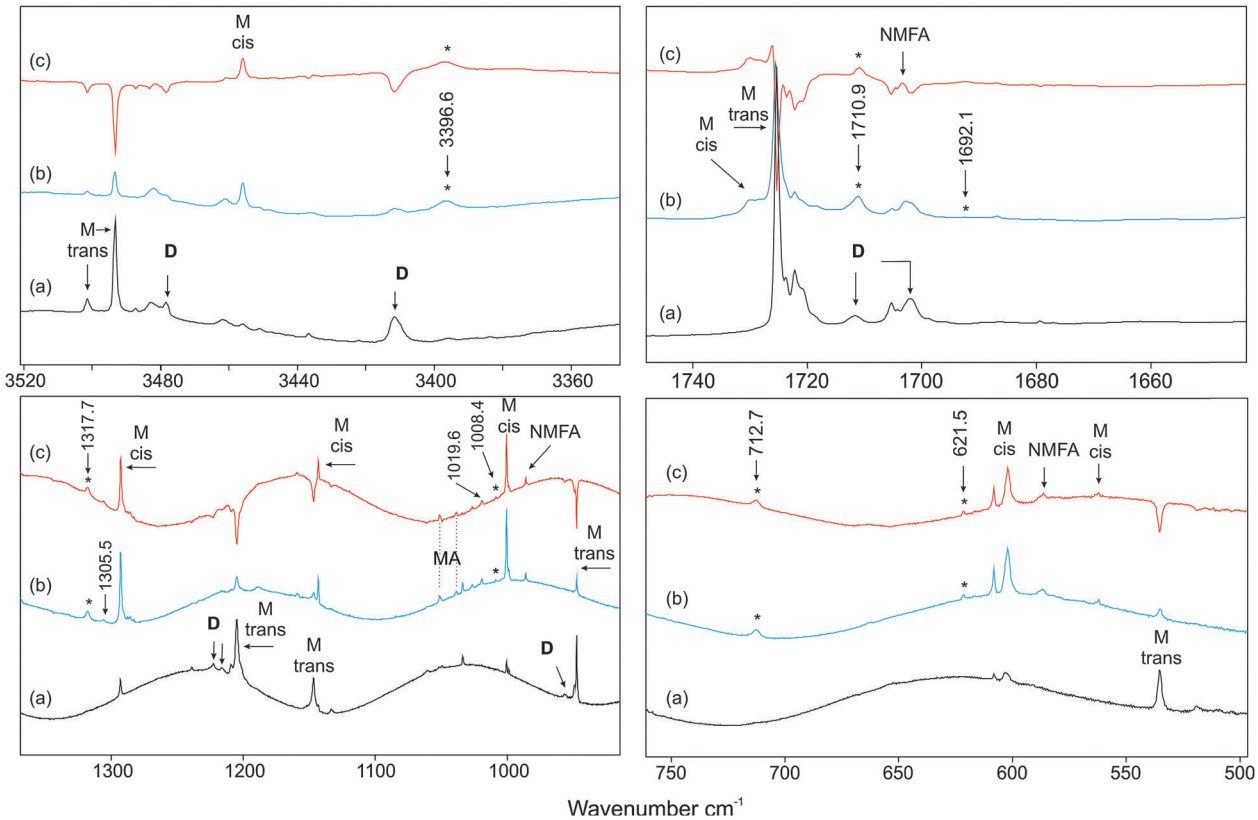

Fig. 3 (a) Matrix-isolated IR spectrum of NMF in argon matrix at 10 K, the sample temperature during deposition was kept at 253 K. (b) Matrix-isolated IR spectrum of NMF in argon at 10 K after 30 minutes irradiation at λ = 248 nm. (c) Matrix-isolated difference spectrum of NMF in argon at 10 K after 30 minutes irradiation at λ = 248 nm. Bands of monomeric NMF are marked M, D bands were assigned to the ***tt-1*** and ***tt-2*** dimers, the bands assigned to the ***tc-3*** and ***tc-4*** dimers are highlighted (*), bands of the *N*-methylformimidic acid are marked as NMFA, and bands of the methylamine are marked MA.

between the two sets of data is only 0.2 eV, with a maximum deviation of 0.4 eV. The order of localized and CT states is the same with both methods. The selection of the long-range separation parameter μ is one important issue influencing the performance of long range-corrected functionals, as the relative position of localized and especially CT states are very affected by the value of μ.[24,36]

The energies of the two first excited states (nπ*(A) and nπ*(B)) at the TD-DFT level are about 5.4 eV and 5.6 eV for all dimers (Table 4). For the ***tt-1*** isomer the excitation energies calculated at the MS-PT2//CASSCF(14,10)/aug-cc-pVDZ level of theory are 5.6 and 5.8 eV, which are 0.2 eV shifted with respect to the TDDFT values. The energy of these states does not depend on the geometry or conformational changes between the monomers because of their local nature. At TDDFT, the nπ* excited states of the *cis* and *trans* monomers have energies of 5.42 eV and 5.52 eV respectively. The corresponding MS-PT2 values are 5.93 and 6.00 eV; and the value reported by Serrano-Andrés and Fuelscher for the lowest excitation energy of the *trans* monomer at CASPT2 level with a TZV-quality basis set including Rydberg type functions is 5.52 eV.[38]

For ***tt-1*** and ***tt-2***, the excited states S_3 to S_5 are related to excitations from localized orbitals in one of the monomers to very diffuse orbitals of Rydberg nature. In the case of the S_3 and S_4 states, important contributions of electronic transitions from the n(A) orbital to the LUMO (more than 30%) are found. The LUMO is a Rydberg orbital (3p) from monomer B (Fig. 5S, ESI†), which implies an important electron transfer from A to B. Consequently, the S_3 and S_4 states can be classified as CT(A → B). In the case of S_5, the initial orbital is the lone pair localized on B (n(B)). Thus, this is a local excitation on monomer B involving a diffuse orbital.

The good agreement between the TDDFT and the ADC(2) methods indicates that these states are real and not artifacts due to an improper DFT description. There are additional evidences showing that the Rydberg states of the isolated molecule are in this spectral region. Serrano-Andres and Fuelscher reported the 3s-Rydberg state with an excitation energy of 6.08 eV (CASPT2 and TZVP and diffuse functions) in *trans* NMF.[38] These states, however, were not obtained in previous studies of similar systems performed with a smaller basis set without diffuse functions.[13,14,21]

To analyze the effect of the argon matrix on the excited-states energies, the excited states of the ***tt-1*** and ***tt-2*** isomers were computed considering the argon matrix with a continuum model (argon dielectric constant = 1.430). The order of the states did not change with respect to the gas-phase calculations and the effect on the LE(A) and LE(B) energies is smaller than 0.1 eV, while for the CT is around 0.1 eV (Table S4, ESI†). The small impact of the matrix on the electronic structure of the chromophore was also observed in our previous calculations on

Table 4 Vertical excitations (E) and oscillator strengths (f) calculated at the TD/LC-BLYP(μ = 0.2)/6-311+G(d) and ADC(2)/aug-cc-pVDZ levels of theory for the ***tt-1***, ***tt-2***, ***tc-3*** and ***tc-4*** isomers. The geometries were obtained at the B3LYP-D3/aug-cc-pVTZ level of theory. Ryd – Rydberg; LE – local excitation; CT – charge transfer

	TD-DFT		ADC(2)		
	E (eV)	f	E (eV)	f	Character
tt-1					
S_1	5.43	0.002	5.50	0.001	nπ*(A), LE(A)
S_2	5.61	0.002	5.66	0.001	nπ*(B), LE(B)
S_3	5.80	0.003	5.87	0.008	n(A) → Ryd, CT(A → B)
S_4	5.83	0.004	6.03	0.006	n(A) → Ryd, CT(A → B)
S_5	6.07	0.002	6.22	0.005	n(B) → Ryd; LE(B)
tt-2					
S_1	5.46	0.004	5.51	0.003	nπ*(A), LE(A)
S_2	5.70	0.001	5.72	0.001	nπ*(B), LE(B)
S_3	5.74	0.003	5.77	0.011	n(A) → Ryd, CT(A → B)
S_4	5.81	0.013	5.94	0.003	n(A) → Ryd, CT(A → B)
S_5	6.04	0.001	6.21	0.002	n(B) → Ryd; LE(B)
tc-3					
S_1	5.46	0.004	5.52	0.002	n-π*(A), LE(A)
S_2	5.61	0.001	5.60	0.000	n-π*(B), LE(B)
S_3	5.79	0.014	5.77	0.013	n(A) → Ryd, CT(A → B)
S_4	5.82	0.002	5.97	0.000	n(A) → Ryd, CT(A → B)
S_5	6.00	0.001	6.41	0.000	n(A) → π*(B), CT(A → B)
tc-4					
S_1	5.43	0.003	5.50	0.002	n-π*(A), LE(A)
S_2	5.62	0.001	5.60	0.000	n-π*(B), LE(B)
S_3	5.80	0.009	5.82	0.010	n(A) → Ryd, CT(A → B)
S_4	5.86	0.000	6.02	0.001	n(A) → Ryd, CT(A → B)
S_5	5.99	0.002	6.40	0.000	n(A) → π*(B), CT(A → B)

the monomer at QM/MM level of theory,[2] which did not show any significant effect of the matrix on the excited states energies. The main effect of the matrix was to create a cage that helped the recombination process.

Excited states: reaction pathways. To investigate the deactivation pathways of the N–H···O=C *trans–trans* dimers, three crossing points between S_0 and S_1 were explored. They are associated to the main nonradiative deactivation channels of the ***tt-1*** dimer: CN dissociation in monomer A (CN-A), CN dissociation in monomer B (CN-B), and proton transfer between A and B (PT). The CN-A and CN-B pathways, also present in the monomer,[2] correspond to relaxations in the nπ*(A) and nπ*(B) states and the proton-transfer pathway is associated to the relaxation in the CT(A → B) state. The S_1/S_0-crossing geometries for these three pathways are shown in Fig. 4. We will discuss later that non-adiabatic dynamics simulations showed that these intersections are relevant during the deactivation of ***tt-1*** and that equivalent structures are observed for ***tt-2*** as well.

The CN-A and CN-B intersections have very similar geometries to those previously found for the monomers, the C–N distance in the dissociated monomer is about 2.5 Å (Fig. 4a and b). Reflecting the local nature of the corresponding excited state, the geometry of the other monomer is not significantly affected with respect to the ground-state minimum geometry. At the crossing, the intermolecular distance between the donor and the acceptor slightly decreases in comparison to the

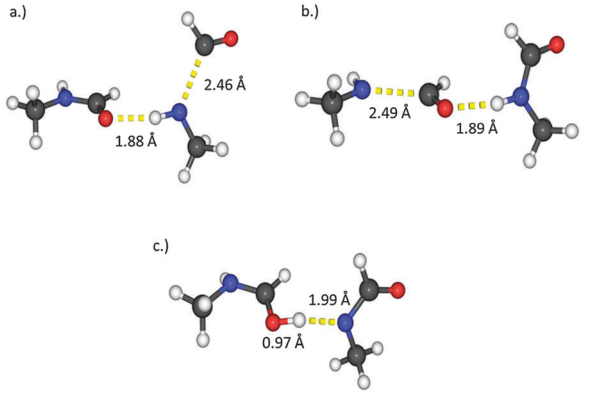

Fig. 4 S_1/S_0 intersection geometries. (a) CN-A dissociation crossing. (b) CN-B dissociation crossing. (c) PT crossing.

ground state minimum, due to the higher donor and acceptor capacities of the radical species. As it was found for the isolated monomers,[2] the CN-A and CN-B crossings have larger energies than the corresponding S_1 minima in the excited state.

The crossing associated to the proton-transfer process (Fig. 4c) has a comparable geometry to those previously reported for similar systems.[13] The donor monomer remains almost planar, while the N atom of the acceptor pyramidalizes. The O–H distance is 0.97 Å and the N···H intermolecular distance is around 2 Å. The PT crossing is more stable than the corresponding CN-bond-breaking crossings by at least 1.5 eV (at all levels of theory).

To analyze the shape of the potential energy surfaces along the main reaction coordinates, energy profiles were built with linear interpolation of internal coordinates (LIIC).

To build the LIIC energy profile for the PT channel of ***tt-1***, the S_0 minimum, the transition state (TS) along the S_1 PT path, and the PT crossing were used. The S_0 minimum was optimized with MP2/aug-cc-pVDZ, the S_1 TS was optimized with ADC(2)/aug-cc-pVDZ, and the PT crossing was also obtained with ADC(2) by optimizing the S_1 state until the crossing was reached. LIIC geometries were created between S_0 minimum and TS, and between TS and the PT crossing. ADC(2) and TDDFT single-point calculations were done for this set of geometries. The results are shown in Fig. 5.

In the case of the CN-breaking channel of ***tt-1***, LIIC energy profiles were built between the S_0 minimum and the CN-dissociation crossings in monomers A and B. Single point energies were then computed with MS-PT2, ADC(2) and TDDFT. These results are shown in Fig. 6 for CN dissociation in both monomers. LIIC between the S_1 minimum and all crossings are shown in Fig. 6S–8S of the ESI.†

The energy profile along the PT channel (Fig. 5) connects the Franck–Condon region to the PT crossing through a shallow S_1 minimum and a relatively small energy barrier of about 0.3 eV. This barrier is approximately at the same level as the S_1 energy at the Franck–Condon point. A good agreement is observed between ADC(2) and TDDFT results.

For CN breaking, the energy profiles show an increasing of the S_1 energy up to the top of a barrier, from where it decreases

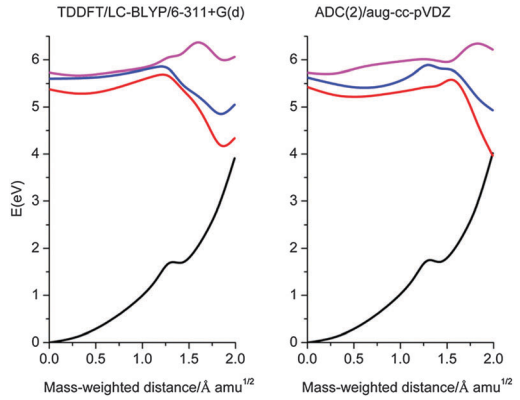

Fig. 5 Potential energy profile between the S_0 geometry and the crossing geometry for the proton-transfer process in dimer ***tt-1*** optimized at the ADC(2) level of theory.

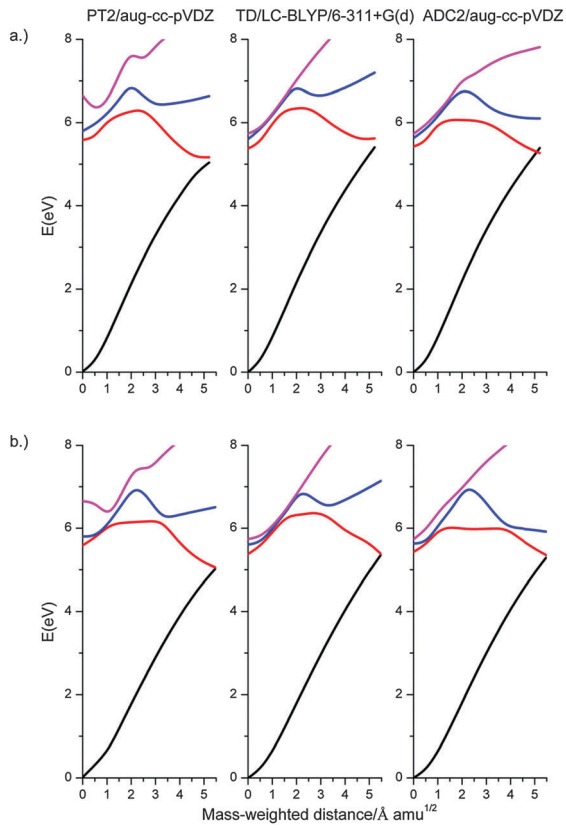

Fig. 6 Potential energy profile between the S_0 geometry and the crossing geometry for the CN-breaking process in dimer ***tt-1***. (a) Monomer A (CN-A) in dimer ***tt-1***. (b) Monomer B (CN-B).

until finding the CN-dissociation crossing. The comparison between the three energy profiles also shows a good agreement between all three methods.

The degree of distortion and the reaction barriers indicate that the PT channel should be more important for the deactivation of the dimers than the CN dissociation. On the other hand, since the barriers for both processes are of the same order of magnitude, some competition is expected. Non-adiabatic dynamics simulations were performed to analyze this competition and to understand the underlying relaxation mechanism at the initial steps of the process. These results are discussed in the next section.

Non-adiabatic dynamics. Non-adiabatic dynamic simulations were performed for the ***tt-1*** and ***tt-2*** isomers. To generate the initial conditions, the absorption spectra were computed with the nuclear ensemble approach[39,40] based on 500 geometries sampled according to a Wigner distribution for the harmonic oscillator. Normal modes were calculated at the LC-BLYP/6-311+G(d) level of theory. To simulate the excitation with the wavelength of the 248 nm laser, initial conditions were picked from an energy window of 0.5 eV centered at 5.0 eV. The initial state of the trajectories was statistically distributed among S_1, S_2 and S_3, according to the oscillator strengths of each point to be excited into each state. The number of trajectories starting in each state for both sets of simulations is given in Table 5. The character of the initial state in terms of charge transfer and localization plays a central role on the reaction mechanism and it will be discussed below.

The computed trajectories decayed to the ground state according to two different mechanisms: (1) relaxation in the CT(A → B) state inducing proton transfer (PT channel); and (2) relaxation in the local nπ* states inducing CN dissociation (CN channel). This could happen either in monomer A (CN-A) or in B (CN-B), depending on where the excitation is located. These mechanisms involve the crossings between S_1 and S_0 discussed above (Fig. 4).

Table 5 shows the distribution of the trajectories following PT and CN channels for both isomers. The most important channel was PT with 72% of the trajectories of ***tt-1*** and 55% of ***tt-2***. The other trajectories deactivated through the CN channels. The PT channel was predominantly activated for trajectories starting in S_3, while the importance of the CN channel increased for trajectories starting in S_1. In the case of ***tt-1***, 96% of the CN trajectories followed the CN-A channel (dissociation of monomer A), and the remaining 4% followed the CN-B channel. For ***tt-2***, CN trajectories equally split between CN-A and CN-B channels.

The distribution of decay times, as given for a 0.1 eV threshold (see Computational details), can be fitted with a single exponential decay function (see Fig. 9S of the ESI†)

$$f(t) = \exp[-(t - \tau_d)/\tau_e],$$

Table 5 Non-adiabatic dynamics simulations for ***tt-1*** and ***tt-2*** isomers: number of trajectories starting in each state (#trajectories) and distribution of trajectories between the PT and CN channels

	S_1	S_2	S_3	Total
Dimer ***tt-1***				
# trajectories	20	11	19	50
% PT	50	92	89	72
% CN	50	8	11	28
Dimer ***tt-2***				
# trajectories	19	20	12	51
% PT	42	65	67	55
% CN	58	35	33	45

Table 6 Time constants for the decay to S_0 from the non-adiabatic dynamics results

	τ_d (fs)	τ_e (fs)	$\tau = \tau_d + \tau_e$ (fs)	τ_{PT} (fs)
tt-1				
PT	15	64	79	36
CN	131	176	307	—
Total	12	108	121	—
tt-2				
PT	23	115	138	54
CN	38	230	268	—
Total	24	170	194	—

where τ_d is the latency time to start the deactivation and τ_e is the exponential decay constant. The excited-state lifetime τ is given by the sum of τ_d and τ_e (Table 6). Both isomers deactivate in the ultrafast scale, ***tt-1*** within 121 fs and ***tt-2*** within 194 fs. Trajectories following the PT channel tend to decay relatively faster than trajectories following the CN channel.

The initial conditions were examined to understand the differences between ***tt-1*** and ***tt-2*** and to check whether they affected the distribution of different channels. While the three excited states considered in the dynamics are very close in energy and there are transitions between them during the processes, we found out that the nature of the excited state at the beginning of the dynamics has certain influence in the population of each particular reaction channel. The analysis of the charge-transfer amount in the initial state at time 0 shows that with a large degree of charge transfer, the trajectory tends to decay through the proton transfer mechanism (Fig. 10S and 11S, ESI†). The average A → B initial charge-transfer degree in PT trajectories is 0.2*e* (*e* – electron charge) larger than in the CN trajectories. In particular, the distributions between the CN-A and CN-B channels are very dependent on the initially populated state. For the CN trajectories, the analysis of TXT(A) parameter,[36] which provides a measure of the localization of the electron density during electronic excitation, shows that 90% of the CN-B trajectories started on a nπ*(B) state and that 79% of the CN-A trajectories are associated to the nπ*(A) state (Fig. 12S, ESI†).

In the PT trajectories, the proton is transferred very quickly, within an average time of 36 fs and 54 fs for ***tt-1*** and ***tt-2*** respectively (τ_{PT} in Table 6; the evolution of mean value of the O–H and N–H distances in the ***tt-1*** set is shown in Fig. 7d). Then, the dimer oscillates around the CT(A → B) minimum before it decays to the ground state. Since the tautomer is not stable, the initial structure is recovered.

For a single selected PT-channel trajectory in the ***tt-1*** set, Fig. 7a–c shows the evolution of the potential energies, N–H and O–H distances, and the excess of electronic charge, fraction of proton charge and net charge in monomer B. This specific trajectory was chosen for this analysis because it shows the main aspects generally observed in the PT trajectories in a very short time. The excess of electronic charge in the excited state was computed using the method described in ref. 27. The fraction of proton charge in monomer B was taken proportional to the OH distance, varying between 0 and 1 between the maximum and the minimum OH distance. The net charge is given as the sum of the excess of electronic charge and the fraction of proton charge.

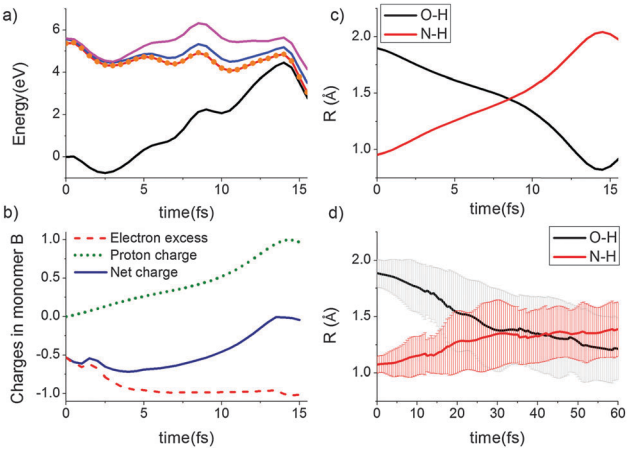

Fig. 7 (a–c) Example of a proton-transfer trajectory (***tt-1***): (a) evolution of potential energy (dots indicate the current state); (b) charges in monomer B during the dynamics; (c) N–H and O–H distances; (d) evolution of the average N–H and O–H distances for the first 60 fs in the dynamics of PT trajectories (***tt-1***). Dashed areas indicated the standard deviation.

For this trajectory, the simulation started in an excited state with a significant degree of A → B charge-transfer character (around 0.5*e*). The electron transfer increases with the time and reaches approximately 1*e* after 6 fs. At this point, the proton still belongs to monomer A, but it quickly follows the electron and transfers to monomer B. Near the crossing point, the net charge of monomer B is zero, implying that a full hydrogen atom was finally transferred.

The important role of the charge-transfer state in the PT channel requires the use of long-range corrected functionals for a proper description of this kind of processes at the TDDFT level. We have tested the dynamics simulations using other functionals and it was clear that the final distribution of trajectories between the CN and PT channels was very much correlated to the amount of Hartree–Fock exchange in the functional.

This kind of hydrogen-transfer protective mechanism seems to be general in the UV-deactivation of biological building blocks.[1] Another model system, the formic-acid dimer, which is used as a prototype for DNA base pairs,[41–44] was studied by Novak *et al.*[41] They analyzed singly and doubly hydrogen-bonded formic-acid dimers using non-adiabatic dynamics and found the single and double proton-transfer channel as the main deactivation mechanisms and no fragmentation, also in contrast to the dissociative photochemistry of the monomer.

Similar to the dynamics of NMF monomer,[2] the CN channel in the dimers requires an initial relaxation to one of the S_1 CN minima. This mechanism involves a fast population of S_1 (at 60 fs, 80% of the trajectories have already decayed to S_1; Fig. 9S, ESI†). Then, the molecule relaxes to one of the S_1 CN minima. These minima are characterized by pyramidalization of the N and enlargement of the C–N distance. (In ref. 2, we discuss how

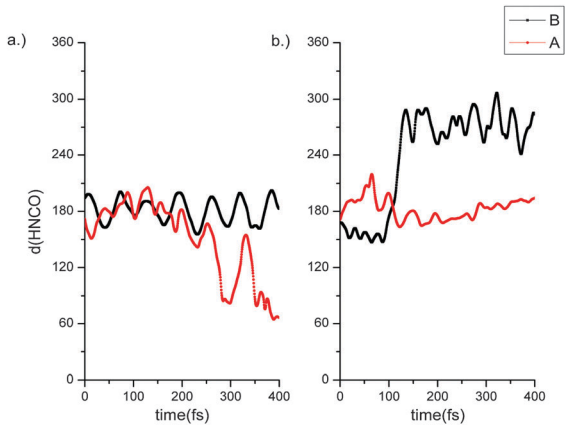

Fig. 8 Evolution of the HNCO angles of A and B monomers in two characteristic trajectories: (a) CN-A trajectory; (b) CN-B trajectory.

these deformations are needed for the formation of the radical pairs and how they are related to the isomerization pathway.)

The relaxation to the S_1 CN minimum takes about 200 fs, which explains the longer lifetimes of CN channel compared to PT channel (Table 6). One interesting feature observed in the CN trajectories is that only one of the monomers relaxes to the S_1 minimum, while the other remains oscillating around the ground state geometry; reflecting the local nature of the excited state. This feature is illustrated for two selected trajectories in Fig. 8, in terms of the time evolution of the HNCO angles in each monomer. Similar graph including all CN-channel trajectories is shown in the ESI,† Fig. 13S.

We previously characterized four minima of the NMF monomer in the nπ* excited state: three have a *cis* geometry, while one has *trans* geometry.[2] We looked for analogous structures in the ***tt-1*** dimer, but due to the second NMF molecule, only five complexes were found (eight minima were expected considering four for each monomer). The most stable structure is related to the relaxation of the A monomer, with geometry very similar to the ***tc-1*** dimer. This minimum is 0.2 eV more stable than the all minima related to the relaxation of the B monomer. This enhanced stability of the S_1 CN-A minima helps to rationalize why almost all ***tt-1*** CN trajectories dissociated in monomer A.

The competition between the CN and PT channels is related to the distribution of kinetic energy between different modes in the excited state, while the PT channel is faster and can be easily accessed with small deformations from the initial structure, in some cases the dimer still relaxes to one of the CN minima. When that happens, the CN channel is activated.

In this work, we did not consider the effect of the matrix in the simulations. We expect that a significant fraction of dissociated trajectories should recombine under matrix conditions. In the case of the monomer, we predicted 28% of recombination in the argon matrix.[2] In addition, the hydrogen-bonded structure of the dimer is expected to induce a larger percentage of recombination. To understand the final distribution of products, longer simulation times are required, and the matrix environment should be explicitly considered.

Discussion: isomerization

On one hand, our experimental results revealed that irradiation of *trans–trans* dimers with 248 nm light produces the ***tc-3*** and ***tc-4*** dimers as main products (reactions 1 and 2). As already mentioned, this indicates that *trans–cis* isomerization may be restricted to monomer B. On the other hand, our simulations show significant differences between the photochemistry of dimers and the monomer, since the deactivation of the dimer takes place mainly *via* a proton-transfer mechanism. However, these simulations do not explain the preference for isomerization in one of the monomers. In this context, the isomerization of only monomers B needs further consideration.

One first possibility is that ***tc-3*** and ***tc-4*** are formed not by exclusive isomerization of monomer B, but by further reorganization of the dimers. This is, however, unlikely because the ***tc-3*** and ***tc-4*** isomers are not the most stable of the *trans–cis* systems.

Another possibility is that there is an energetic preference for isomerizing one or other monomer. Rotational barriers were computed in the ground (LC-BLYP(μ = 0.2)/6-311+G(d)) and the first excited states (TD/LC-BLYP(μ = 0.2)/6-311+G(d)). In the ground state, transition-state calculations were carried out releasing all degrees of freedom. For the excited state, the O═C–N–H dihedral angle was fixed at the ground-state value and the remaining variables were allowed to relax.

The rotational barriers corresponding to the ***tt-1*** isomer in the ground state are 23.5 and 25.2 kcal mol^{-1} for the rotation of A and B monomers respectively (Table 7). These values are very similar but slightly higher than the barrier for the rotation in the isolated monomer (22.2 kcal mol^{-1}), because of a small steric hindrance in the dimers. The small advantage of A over B does not justify a selective rotation of one of the monomers in the ground state, unless there is an energy transfer of this magnitude from A to B. For the first excited state, the barriers are reduced to 0.8 and 1.4 kcal mol^{-1} respectively (the process should be barrierless after relaxing all degrees of freedom). Thus, there are no energetic preferences to isomerize either one or other monomer either in the ground or in the excited states.

A third possibility is that the preference for B isomerization could be related to deactivation at the CN channel followed by recombination, rather than to the PT channel. In fact, exclusive rotation of monomer B could be achieved if initially only the nπ*(B) were populated. However, nπ*(A) and nπ*(B) are very

Table 7 Transition-state energies for the *trans–cis* isomerization in S_0 and S_1

Molecule	Isomerization	ΔE_{TS} (kcal mol^{-1}) S_0	S_1
tt-1	Monomer A	23.5	0.8
tt-1	Monomer B	25.2	1.4
trans	Monomer	22.2	1.3
$[CH_3–NH–C═OH]^{\bullet}$	Monomer B (radical)	4.6	—
$[CH_3–NH–C═OH]^{+}$	Monomer B (cation)	46.7	—
$[CH_3–NH–C═O]^{\bullet}$	Monomer A (radical)	3.2	—
$[CH_3–NH–C═O]^{-}$	Monomer A (anion)	26.3	—

close in energy (Table 4) and if any bias would be expected from this factor, it would favor A isomerization, which is slightly lower in energy. In their work on the glycine dimer, Marazzi *et al.* proposed a mechanism to transfer energy from the nπ*(A) to the nπ*(B) through an avoiding crossing between these states found along the $NC_\alpha C_\beta O$ improper torsion angle. They suggested that this mechanism is unlikely due to the small coupling between the states and the small oscillator strength of the nπ*(A) state. We did not find evidences of this mechanism in our non-adiabatic simulations.

A fourth possible mechanism could be related to the relaxation in the CT state, with the isomerization happening at the proton-transferred species before the back proton transfer, and with selective isomerization of B induced by energy transfer from A to B during the proton transfer.

To check this possibility, we computed the ground-state *trans–cis* isomerization barrier for the isolated $[CH_3–NH–C{=}OH]^\bullet$ and $[CH_3–NH–C{=}O]^\bullet$ radicals and for the isolated $[CH_3–NH–C{=}OH]^+$ and $[CH_3–NH–C{=}O]^-$ ions, which are the species formed after the proton transfer. Inspection of these barriers in Table 7 immediately shows that isomerization of the ionic species can be discarded, as they need at least 26.3 kcal mol^{-1} to isomerize the anion and 46.7 kcal mol^{-1} to isomerize the cation. Isomerization of the radicals, however, is feasible upon overcoming a barrier of 3.2 kcal mol^{-1} in the proton donor (A) or 4.6 kcal mol^{-1} in the proton acceptor (B).

Additionally, the dynamics simulations showed that there is an energy transfer from A to B during the proton transfer. An average gain of 14 kcal mol^{-1} of kinetic energy on the monomer B was observed for the PT trajectories, being 5 kcal mol^{-1} delivered by the transferred proton and the remaining coming from potential-energy stabilization.

Although we cannot definitively provide a final explanation for the selective isomerization of B, isomerization of the radical induced by a surplus of energy in B seems to be a viable source for this phenomenon.

Conclusions

Hydrogen-bonded molecules in biological systems, in particular peptides and proteins, are frequently exposed to UV irradiation. A better understanding of how hydrogen bonding affects the photochemistry of these molecules requires unraveling the deactivation mechanisms after UV-irradiation. In contrast to the photochemistry of the isolated monomer of NMF, which undergoes photo-dissociation, we showed in this work that the dimer is stable towards irradiation.

Dimers of NMF serve here as simple models for hydrogen-bonded peptides with *trans–cis* isomerism. While *trans*-NMF is thermodynamically more stable than *cis*-NMF, the *cis* isomer can form more stable dimers, since both the C=O group as hydrogen bond acceptor and the N–H group as hydrogen bond donor point to the same side of the molecule and thus can both be involved in hydrogen bonding with a second molecule of NMF. Dimers involving *cis*-NMF could be conveniently produced by 248 nm irradiation of the ***tt*** dimers. In this process only the hydrogen-bond acceptor monomer (B) isomerizes.

Reaction pathways and non-adiabatic dynamics simulations reveal that non-adiabatic decay to the ground state could occur through two different mechanisms, proton-transfer through a CT state or CN relaxation on the nπ* state of either monomer. Both processes are ultrafast but the proton-transfer is significantly faster because it can be easily activated through small deformations from the Franck–Condon geometry.

Also for this reason, proton transfer is the predominant deactivation channel. It is characteristically photo-stable, returning to the initial reactants after the internal conversion, which explains the observed photo-stability of the dimers compared to monomers.

In our simulations, the CN mechanism was activated when the dimers relaxed into the nπ*(A) or nπ*(B) states before the CT state was populated. The CN mechanism does not necessary produce the dissociative products, but it is the initial step for various processes that take place in the monomer such as CN breaking, formation of amide···CO complexes, isomerization, and recombination.

The reason of the selective isomerization in B isomer is still not fully understood and deserves further investigation. A number of possible mechanisms, such as selective population of nπ*(B) or energy transfer to the proton acceptor during the proton-transfer process, were considered and discussed.

Acknowledgements

E. S.-G acknowledges a Liebig-stipend from the Fonds der Chemischen Industrie. This work was supported by the Cluster of Excellence RESOLV (EXC 1069) funded by the Deutsche Forschungsgemeinschaft.

References

1 A. L. Sobolewski and W. Domcke, *Phys. Chem. Chem. Phys.*, 2010, **12**, 4897.
2 R. Crespo-Otero, A. Mardyukov, E. Sanchez-Garcia, M. Barbatti and W. Sander, *ChemPhysChem*, 2013, **14**, 827.
3 I. Antol, M. Eckert-Maksic, M. Barbatti and H. Lischka, *J. Chem. Phys.*, 2007, **127**, 234303.
4 M. Ruzi and D. T. Anderson, *J. Chem. Phys.*, 2012, **137**, 194313.
5 R. Ludwig, F. Weinhold and T. C. Farrar, *J. Chem. Phys.*, 1997, **107**, 499.
6 J. M. M. Cordeiro, M. A. M. Cordeiro, A. R. S. A. Bosso and J. R. S. Politi, *Chem. Phys. Lett.*, 2006, **423**, 67.
7 M. Albrecht, C. A. Rice and M. A. Suhm, *J. Phys. Chem. A*, 2008, **112**, 7530.
8 E. M. Kosower, G. Markovich and G. Borz, *J. Phys. Chem. B*, 2009, **113**, 5622.
9 S. Shin, A. Kurawaki, Y. Hamada, K. Shinya, K. Ohno, A. Tohara and M. Sato, *J. Mol. Struct.*, 2006, **791**, 30.
10 D. Shemesh, A. L. Sobolewski and W. Domcke, *J. Am. Chem. Soc.*, 2009, **131**, 1374.

11 D. Shemesh, A. L. Sobolewski and W. Domcke, *Phys. Chem. Chem. Phys.*, 2010, **12**, 4899.
12 M. Malis, Y. Loquais, E. Gloaguen, H. S. Biswal, F. Piuzzi, B. Tardivel, V. Brenner, M. Broquier, C. Jouvet, M. Mons, N. Doslic and I. Ljubic, *J. Am. Chem. Soc.*, 2012, **134**, 20340.
13 M. Marazzi, U. Sancho, O. Castano and L. M. Frutos, *Phys. Chem. Chem. Phys.*, 2011, **13**, 7805.
14 M. Marazzi, I. Navizet, R. Lindh and L. M. Frutos, *J. Chem. Theory Comput.*, 2012, **8**, 1351.
15 A. L. Sobolewski and W. G. Domcke, *J. Phys. Chem. A*, 2007, **111**, 11725.
16 M. Barbatti, *Wiley Interdiscip. Rev.: Comput. Mol. Sci.*, 2011, **1**, 620.
17 M. Barbatti, J. Pittner, M. Pederzoli, U. Werner, R. Mitric, V. Bonacic-Koutecky and H. Lischka, *Chem. Phys.*, 2010, **375**, 26.
18 F. Plasser, M. Barbatti, A. J. A. Aquino and H. Lischka, *Theor. Chem. Acc.*, 2012, **131**, 1073.
19 B. F. E. Curchod, U. Rothlisberger and I. Tavernelli, *ChemPhysChem*, 2013, **14**, 1314.
20 S. Grimme, S. Ehrlich and L. Goerigk, *J. Comput. Chem.*, 2011, **32**, 1456.
21 M. Marazzi, U. Sancho, O. Castano, W. Domcke and L. M. Frutos, *J. Phys. Chem. Lett.*, 2010, **1**, 425.
22 A. Dreuw, J. L. Weisman and M. Head-Gordon, *J. Chem. Phys.*, 2003, **119**, 2943.
23 Y. Tawada, T. Tsuneda, S. Yanagisawa, T. Yanai and K. Hirao, *J. Chem. Phys.*, 2004, **120**, 8425.
24 T. Minami, M. Nakano and F. Castet, *J. Phys. Chem. Lett.*, 2011, **2**, 1725.
25 C. Hattig, in *Advances in Quantum Chemistry: A Tribute to Jan Linderberg and Poul Jorgensen*, ed. J. R. Sabin and E. Brandas, Elsevier Academic Press Inc, San Diego, 2005, vol. 50, p. 37.
26 A. B. Trofimov and J. Schirmer, *J. Phys. B: At., Mol. Opt. Phys.*, 1995, **28**, 2299.
27 R. Crespo-Otero and M. Barbatti, *Theor. Chem. Acc.*, 2012, **131**, 1237.
28 J. C. Tully, *J. Chem. Phys.*, 1990, **93**, 1061.
29 G. Granucci and M. Persico, *J. Chem. Phys.*, 2007, **126**, 134114.
30 F. Aquilante, L. D. Vico, N. Ferré, G. Ghigo, P.-Å. Malmqvist, P. Neogrády, T. B. Pedersen, M. Pitonak, M. Reiher, B. O. Roos, L. Serrano-Andrés, M. Urban, V. Veryazov and R. Lindh, *J. Comput. Chem.*, 2010, **31**, 224.
31 R. Ahlrichs, M. Bar, M. Haser, H. Horn and C. Kolmel, *Chem. Phys. Lett.*, 1989, **162**, 165.
32 M. J. Frisch, G. W. Trucks, H. B. Schlegel, G. E. Scuseria, M. A. Robb, J. R. Cheeseman, G. Scalmani, V. Barone, B. Mennucci, G. A. Petersson, H. Nakatsuji, M. Caricato, X. Li, H. P. Hratchian, A. F. Izmaylov, J. Bloino, G. Zheng, J. L. Sonnenberg, M. Hada, M. Ehara, K. Toyota, R. Fukuda, J. Hasegawa, M. Ishida, T. Nakajima, Y. Honda, O. Kitao, H. Nakai, T. Vreven, J. A. Montgomery, Jr., J. E. Peralta, F. Ogliaro, M. Bearpark, J. J. Heyd, E. Brothers, K. N. Kudin, V. N. Staroverov, R. Kobayashi, J. Normand, K. Raghavachari, A. Rendell, J. C. Burant, S. S. Iyengar, J. Tomasi, M. Cossi, N. Rega, N. J. Millam, M. Klene, J. E. Knox, J. B. Cross, V. Bakken, C. Adamo, J. Jaramillo, R. Gomperts, R. E. Stratmann, O. Yazyev, A. J. Austin, R. Cammi, C. Pomelli, J. W. Ochterski, R. L. Martin, K. Morokuma, V. G. Zakrzewski, G. A. Voth, P. Salvador, J. J. Dannenberg, S. Dapprich, A. D. Daniels, Ö. Farkas, J. B. Foresman, J. V. Ortiz, J. Cioslowski and D. J. Fox, *Gaussian 09, Revision A.02*, Gaussian, Inc., Wallingford, CT, 2009.
33 M. Barbatti, *Wiley Interdiscip. Rev.: Comput. Mol. Sci.*, 2011, **1**, 620.
34 M. Barbatti, G. Granucci, M. Ruckenbauer, F. Plasser, R. Crespo-Otero, J. Pittner, M. Persico and H. Lischka, *NEWTON-X: a package for Newtonian dynamics close to the crossing seam*, 2013, www.newtonx.org.
35 F. Plasser, R. Crespo-Otero, M. Pederzoli, J. Pittner, H. Lischka and M. Barbatti, *J. Chem. Theory Comput.*, 2014, **10**, 1395.
36 K. Sen, R. Crespo-Otero, O. Weingart, W. Thiel and M. Barbatti, *J. Chem. Theory Comput.*, 2013, **9**, 533.
37 U. Adhikari and S. Scheiner, *J. Phys. Chem. A*, 2012, **117**, 489.
38 L. Serrano-Andrés and M. Fuelscher, *J. Am. Chem. Soc.*, 1996, **118**, 12190.
39 M. Barbatti, G. Granucci, M. Persico, M. Ruckenbauer, M. Vazdar, M. Eckert-Maksic and H. Lischka, *J. Photochem. Photobiol., A*, 2007, **190**, 228.
40 M. Barbatti, A. J. A. Aquino and H. Lischka, *Phys. Chem. Chem. Phys.*, 2010, **12**, 4959.
41 J. Novak, M. Mališ, A. Prlj, I. Ljubić, O. Kühn and N. Došlić, *J. Phys. Chem. A*, 2012, **116**, 11467.
42 K. Marushkevich, L. Khriachtchev, M. Räsänen, M. Melavuori and J. Lundell, *J. Phys. Chem. A*, 2012, **116**, 2101.
43 K. Marushkevich, M. Siltanen, M. Räsänen, L. Halonen and L. Khriachtchev, *J. Phys. Chem. Lett.*, 2011, **2**, 695.
44 K. Marushkevich, M. Siltanen, M. Räsänen, L. Halonen and L. Khriachtchev, *J. Phys. Chem. Lett.*, 2011, **2**, 695.